89 DEMONSTRATING THE UTILITY OF CONDITIONAL PROBABILITIES OF TORNADO DAMAGE RATING IN THE IMPACT-BASED WARNING ERA

Bryan T. Smith[1*], Richard L. Thompson[1], Andrew R. Dean[1], Patrick T. Marsh[1], Richard Wagenmaker[2], Gregory Mann[2], Michael J. Hudson[3], and John T. Ferree[4]

[1]NOAA/NWS/NCEP/Storm Prediction Center, Norman, Oklahoma
[2]NOAA/National Weather Service Forecast Office, Detroit/Pontiac, Michigan
[3]NOAA/NWS/Central Region Headquarters, Kansas City, Missouri
[4]NOAA/NWS/NWSHQ/OCWWS, Norman, Oklahoma

1. Introduction

Recent work by Smith et al. (2012a) demonstrated the relationship of convective modes and supercell mesocyclone strength categories [i.e., weak, moderate, and strong based on mesocyclone nomograms (Andra 1997)] to tornado damage intensity. Thompson et al. (2012) took a step further and affirmed a relationship between supercell rotation strength, the near-storm environment [i.e., the Significant Tornado Parameter (STP) after Thompson et al. 2003; Thompson et al. 2012], and tornado damage intensity. Other recent studies (e.g., LaDue et al. 2012; Smith et al. 2012b; Kingfield et al. 2012; Toth et al. 2013) have sought to demonstrate the relationship between tornado intensity —quantified by EF-scale— and Weather Surveillance Radar – 1988 Doppler (WSR-88D) velocity data. Brotzge et al. (2012) revealed a clear relationship between tornado warning statistics and storm mode, suggesting that a combination of real-time convective mode, associated radar attributes (e.g., mesocyclone strength), and near-storm environment information may contribute to improved situational awareness of tornado impacts.

Recent tornado disasters such as the Joplin, MO, tornado of 22 May 2011, helped spur social science research on tornado warning response (e.g., Ripberger et al. 2014) on how populations assess risk given varying messages regarding the tornado threat. The National Weather Service (NWS) Joplin, MO, tornado assessment (NOAA 2011) recommended exploration of tiered meteorological and impact-based information in tornado warnings. One such example involves several NWS local forecast offices tasked with issuing experimental impact-based warnings (IBWs) for severe thunderstorms and tornadoes (Wagenmaker et al. 2014) designed to convey the hazard magnitude (e.g., tornado) and its conditional and commensurate impact on life and property.

Yet, no formal, science-based techniques have been developed to specifically aid in the IBW tornado warning decision-making process. This study strives to explore this shortage of guidance by building upon previous work (i.e., Smith et al. 2012a, Thompson et al. 2012, Smith et al. 2014) through the development of conditional tornado damage probabilities. Specifically, we demonstrate the utility of combining near-storm environment (e.g., STP) and radar attributes (e.g., convective mode, 0.5° storm circulation strength, radar range and radar sampled height) in an effort to provide real-time probabilistic estimates of tornado damage intensity given the existence of a tornado.

2. Data and Methodology

Radar-based convective modes, peak low-level rotational velocities, and near-storm environment data were assigned to a subset of tornadoes reported in the contiguous United States (CONUS) during 2009-2013. The tornado segment data were filtered by the maximum EF-scale per hour on a 40-km horizontal grid. Archived environmental information (Dean et al. 2006), consisting primarily of supercell-related convective parameters from the hourly SPC objective analyses (Bothwell et al. 2002), accompanied each grid-hour tornado event. Convective mode was assigned by manually examining full volumetric WSR-88D data (Section 2b) at the beginning time of each event. 0.5° peak rotational velocity (V_{rot}) was manually analyzed using super-resolution radar data (Torres and Curtis 2007)

**Corresponding author address:* Bryan T. Smith, NOAA/NWS/NCEP/Storm Prediction Center, 120 David L. Boren Blvd., Suite 2300, Norman, OK 73072. Bryan.Smith@noaa.gov

during the life span of each tornado event (Section 2c). Only tornado events with 0.5° peak V_{rot} documented within 101 mi (≤10,000 ft above radar level) of a WSR-88D were included in this study. The filtering methods resulted in a sample of 4,770 tornado events (Fig. 1) from which conditional tornado probabilities were calculated.

Within the framework described above, the authors made careful manual adjustments to a small portion (7.9%) of the database. Many of the suspected report errors involved incorrectly listed report times, as determined by time-matching the reports to radar data. Examples of this suspected error type included reports well-removed from existing radar echoes and time displaced on the order of tens of minutes to an hour or more. In situations where a suspected error could not be easily corrected, *Storm Data* was used to examine the description of the questionable reports in an effort to identify the storm responsible for the event. Despite alleviating most errors, small time discrepancies on the order of 1-2 volume scans [194 events (51%) of all events exhibiting error had time displacement errors < 10 minutes] were found in *Storm Data* between the beginning time of a tornado event and pertinent WSR-88D velocity signatures, similar to a finding by French et al. (2013) using a mobile radar. Unless a time or location change was necessary based on a well-resolved circulation, we deferred to the NWS documented begin time and location, in an attempt to account for uncertainty and variability in the distance between the tornado location relative to the WSR-88D circulation location (e.g., Speheger and Smith 2006).

a. Quality of SPC hourly mesoscale analyses

The Rapid Update Cycle (RUC; Benjamin et al. 2004) model, and later the Rapid Refresh (RAP) model 0- and 1-h forecasts on a 40-km grid provided the basis for the SPC hourly mesoscale analyses from 2009 through April 2012. Coniglio (2012) evaluated the SPC hourly objective analyses via VORTEX2 field project soundings from the springs of 2009 and 2010 across the Great Plains and found that the SPC analyses improved upon the background 1-h RUC model forecasts of surface temperature and dew point temperature, as well as many derived thermodynamic variables. However, errors were still substantial on occasion (especially above the ground), and large enough to be of concern regarding expected storm evolution. The RUC model was replaced by the RAP model in May of 2012, though comparisons of the RUC and RAP in severe storm environments are lacking in the formal literature. Laflin (2013) examined vertical profiles of temperature and moisture for observed raobs and RAP model soundings and quantified differences in terms of buoyancy [e.g., surface-based convective available potential energy, (SBCAPE)] with a convective-related focus on the preconvective boundary layer. Substantial errors were found in RAP 6- and 12-h forecasts of boundary layer moisture, which resulted in underestimates of buoyancy (e.g., SBCAPE errors around 1000 J kg^{-1}) in dry, well-mixed environments. Yet Laflin (2013) covered only a limited domain (six Great Plains rawinsonde sites) during seven weeks in the late spring 2012, and the findings for longer-range forecasts may not be representative of 0- and 1-h RAP soundings used in the SPC objective analyses, or of other environments supportive of tornadoes (e.g., Thompson et al. 2013).

Potvin et al. (2010) discussed proximity sounding sensitivity to spatiotemporal distance from an event. When examining 0–1 hour proximity sounding data, Potvin et al. (2010) identified a zone within 40–80 km of the launch site (see their Fig. 5) that serves to best characterize the near-storm environment (e.g., minimize convective feedback effects, maintain close distance). The findings of Potvin et al. (2010) were reinforced by Parker (2014), which examined the spatiotemporal variability of VORTEX2 field project soundings relative to both tornadic and nontornadic supercells. Parker (2014) noted that pronounced differences in environmental characteristics extended beyond the storm-induced inflow region, with more favorable combinations of low-level moisture and vertical wind shear evident well away from a small sample of tornadic supercells compared to nontornadic supercells. Still, variability in the near-storm environment was substantial, and a single proximity sounding is not necessarily reflective of supercell tornado potential.

Thompson et al. (2012) found that effective-layer STP (including convective inhibition) exhibited the most utility in discriminating tornado environments as a diagnostic parameter amongst a 39-variable database at the SPC, so results from other parameters are not shown herein. This study utilized the maximum neighborhood grid-hour value within 185 km (100 nm) of each tornado event for STP_1 (hereafter STP_{185km}; Thompson et

al. 2012) to account for proximity concerns and spatial variability of environmental parameters, while providing a relatively simple characterization of the regional tornado environments that were dominated by supercells. The maximum neighborhood approach reflects the ability of the operational meteorologist to consider more than a single grid point value, and to alleviate potential spatial errors in the model-based parameter fields. An example of using the neighborhood grid-hour value versus the grid-hour value is demonstrated by the Rozel, KS, EF4 tornado from 18 May 2013: STP_{185km} reached 4.6 compared to the 40-km grid-hour value of 0.0 in a case with a tornadic storm in proximity to sharp gradients of low-level moisture and buoyancy. Therefore, STP_{185km} is used herein as a single diagnostic to assess tornado potential based on work by Thompson et al. (2012).

b. Radar-based convective mode classification

The Gibson Ridge radar-viewing software (http://www.grlevelx.com/) was used to analyze archived WSR-88D level-II single site radar data (Crum et al. 1993) from the National Climatic Data Center (http://www.ncdc.noaa.gov/nexradinv/) using the closest radar to classify convective mode based on Smith et al. (2012a). Convective mode was determined using full volumetric radar data, especially when data through a deep layer were needed to perform a more thorough assessment of storm structure. Convective mode was assigned based on the volume scan and lower elevation tilts (e.g., 0.5°) of base reflectivity immediately prior to the time of the tornado event. Emphasis herein is placed on the three major convective mode classes of tornadic storms: supercells (3392 events), quasi-linear convective system (894 events), and disorganized cells/clusters and marginal supercells (484 events; hereafter referred to as *other* modes).

Discrete or embedded cells with focused areas of cyclonic (or anticyclonic) azimuthal shear were further scrutinized as potential supercells, following the mesocyclone nomograms developed by the Warning Decision Training Branch of the NWS (after Andra 1997 and Stumpf et al. 1998). Supercells required a peak rotational velocity ≥ 10 m s^{-1} [i.e., a peak-to-peak azimuthal velocity difference of roughly 20 m s^{-1} (40 kt) over a distance of less than 10 km]. Range dependence was included in the mesocyclone designation, per the 1, 2, and 3.5 nm mesocyclone nomograms.

A QLCS is defined as consisting of contiguous reflectivity at or above the threshold of 35 dBZ for a horizontal distance of at least 100 km and a length-to-width aspect ratio of at least 3 to 1 at the time of the event, similar to Trapp et al. (2005). Other modes included disorganized cellular modes that did not include supercell structures (e.g., single cell, multicell), and consisted mainly of conglomerates meeting the reflectivity threshold but not satisfying either supercell or QLCS criteria (e.g., short line segment). Additionally, storms exhibiting transient (i.e., 1-2 volume scans) rotation weaker than the supercell rotation criterion were assigned to the other modes category. For a more thorough discussion pertaining to the complexity and challenges of categorizing convective mode, please refer to Smith et al. (2012a).

c. 0.5° circulation intensity identification

Peak inbound and outbound velocities were examined for each volume scan from immediately prior to tornado formation through tornado dissipation. Only combinations of velocity maxima exhibiting cyclonic (anticyclonic) azimuthal shear within 5 nm and < 45° angle from one another were considered, to avoid primarily convergent or divergent signatures. The maximum 0.5° peak rotational velocity [$V_{rot} = (|V_{in}| + |V_{out}|) / 2$], from all volume scans was assigned to each tornadic event (Fig. 2), and only tornado events sampled at or below 10000 ft above radar level (ARL; <101 mi range) were analyzed and included in this study (Fig. 1). Brief, short-track tornadoes were assigned 0.5° peak V_{rot} immediately prior to the start time for cases not persisting longer than 1 volume scan, whereas longer-lived tornadoes were assigned 0.5° peak V_{rot} from one of the sampling volume scans during the tornado event.

d. Storm-scale rotation considerations

Although the peak V_{rot} only uses a pair of two data points which can be influenced by errors due to aliasing or “noisy data” (Wood and Brown 1997), this dataset considers multiple possible pairs of peak velocity data for individual volume scans during the tornado’s lifetime. This approach can effectively reduce the influence of any volume scan(s) with potential data errors by defaulting to other candidate volume scans. Concerns such as radar beam placement relative to the tornado circulation were partially mitigated by two or more volume scans per tornado event, and the

dependent results of any individual event are likely overwhelmed by the large sample size of tornado events. Underestimates of 0.5° peak V_{rot} owing to beam offset would likely be applied randomly throughout the dataset. Finally, the sampling of circulations by ARL (nearest 100 ft), using the highest radar bin between the two peak V_{rot} data points, was documented in order to account for the effects of radar beam widening with range that reduce the ability of the WSR-88D to resolve storm-scale circulations. Unlike Toth et al. (2013) and LaDue et al. (2012), velocity data were not dealiased manually beyond existing dealiasing algorithm capability for several reasons: 1) our 0.5° peak V_{rot} method is easily reproduced in real-time forecast and warning operations with short time constraints, and 2) the impact of not dealiasing a small fraction of tornado velocity signatures is likely minimized by the large size of this sample (4770 tornado events).

Although tornado circulations appeared to be resolved explicitly in a few cases with large tornadoes close to the radar site, an overwhelming majority of WSR-88D velocity signatures were representative of the larger tornadic vortex (Mitchell et al. 1998) or the low-level mesocyclone (Stumpf et al. 1998). In addition, other classifiable circulations [e.g., mesovortex; Trapp and Weisman (2003)] were also examined. A relatively small percentage of cases (11%) consisted of 0.5° peak V_{rot} diameters exceeding 3.5 mi, which is clearly larger than any documented tornado diameter. While many 0.5° peak V_{rot} cases were easily assessed, 0.5° peak V_{rot} identification at times was a challenging task and involved considerable effort and uncertainty in assigning the peak inbound and peak outbound values. If a tight circulation couplet (i.e., likely resolving the tornado vortex) was clearly separate from other nearby higher velocity bins, the velocity data associated with the smaller-scale circulation were preferentially recorded; otherwise, preference was given to recording velocity information within the larger-scale circulation if the outer circulation V_{rot} value was more than 5 kt greater than the candidate V_{rot} value of the inner circulation.

The manual analysis of velocity data discussed herein is similar to techniques used in real-time warning decision-making. The subjective analysis used to diagnose circulation strength can be advantageous compared to an automated objective approach, especially in cases when radar algorithms do not resolve some tornadic circulations [e.g., landspout; Brady and Szoke (1989)] because of resolution limitations, or when circulations are misidentified along squall lines aligned along the radar beam.

While it was common for velocity signatures to vary during the life cycle of the tornado event, the tornado events in this sample rarely had one outlier volume scan at 0.5° tilt with much stronger V_{rot} (i.e., ≥ 20 kt difference) compared to the other sampled volume scans. Many of the higher-end tornado cases exhibited consistent velocity values that were just below the peak V_{rot} value for several volume scans, including a substantial part of the tornado segment grid hour (i.e., tornado event). Although there was a strong correspondence between the highest EF-scale rating and the maximum 0.5° peak V_{rot}, the two did not necessarily match in time and space. To summarize, 0.5° peak V_{rot} and STP_{185km} are both used as diagnostic variables for estimating the potential tornado damage intensity.

e. Conditional tornado probabilities

Conditional (i.e., upon the occurrence of a tornado) probabilities of tornado intensity, as measured by EF-scale damage, are calculated using STP_{185km} and 0.5° peak V_{rot}. Given the large range in documented STP_{185km} (0-24), 0.5° peak V_{rot} (0-124 kt), and EF-scale (0-5), the sample sizes for paired values of STP_{185km} to EF-scale and 0.5° peak V_{rot} to EF-scale are severely limited in most cases. Therefore, each STP_{185km} value was placed within a bin (e.g., 4.00-5.99), and each 0.5° peak V_{rot} value below 100 kt was placed within a 10 kt bin (e.g., 60.0-69.9 kt).

f. Impact-Based Warnings (IBW)

The IBW tornado damage threat tiers (Table 1) are intended to correspond to tornado intensity (i.e., base, EF0-1; considerable, EF2-5; catastrophic, EF4-5). As of December 2014, 46 NWS local forecast offices are participating in the IBW experiment. At least 10 additional offices will join the IBW experiment in 2015, and nationwide operational implementation is tentatively scheduled for fiscal year 2016.

3. Results and Operational Application

a. Conditional tornado probabilities

While statistically significant differences (α < 0.001) were noted at constant EF-scale between supercells and QLCS modes for both STP_{185km} and 0.5° peak V_{rot} (Smith et al. 2012b), all modes were combined and analyzed together for the sake of brevity. The ability to discriminate between different EF-scale groups diminished at long distance from radar (i.e., range of 70-101 mi. and elevation of 6000'-10000' ARL), especially for the high-end tornado events. However, we have chosen here to combine all event sampling elevations (distances) below 10000' ARL (within 101 nm) for the sake of simplicity.

Acknowledging the aforementioned caveats and characteristics to the underlying data, STP_{185km} and 0.5° peak V_{rot} exhibit utility in discriminating between different EF-scale classes [(e.g., EF0-1, EF2-5, EF4-5), Figs. 3-4]. Conditional probabilities of EF2-5 events slowly increase as STP_{185km} rises in value. The opposite is true for weak (EF0-1) tornadoes. For example, the conditional probability for EF0-1 events and EF2-5 events are 81% and 19%, respectively for the STP_{185km} 3.00-3.99 bin (Fig. 3). The conditional probability of a violent (EF4-5) event becomes nonzero in the 3.00-3.99 STP_{185km} bin threshold. Although the sample sizes become considerably smaller for the higher STP_{185km} bins (e.g., 8.00-9.99), conditional probabilities for EF4-5 events continue to increase through the single digits and into the lower teens for higher values of STP_{185km}.

The 0.5° peak V_{rot} exhibits a substantially stronger signal in discriminating tornado intensity than STP_{185km} as larger 0.5° peak V_{rot} values reveal high conditional probabilities for the stronger EF-scale tornado groups. Conditional probabilities based on 0.5° peak V_{rot} asymptotically approach 0% for EF0-1 events as V_{rot} increases to ≥ 90 kt. The conditional probability for an EF2-5 event becomes the more likely outcome (i.e., 58%) as V_{rot} increases to 60.0-69.9 kt, and violent (EF4-5) tornado damage becomes probable as V_{rot} increases to near 100 kt.

The consideration of both near-storm environment and radar data offers a simple approach when qualitatively "weighing" the influence of each variable for diagnosing estimated tornado intensity. Therefore, a smoothed 2-D plot of STP_{185km} and 0.5° peak V_{rot} was constructed for the conditional probability of an EF2-5 event (Fig. 5; inverse probability of EF0-1 events). The conditional probabilities are more heavily influenced by 0.5° peak V_{rot} than STP_{185km}. For example, when applying a constant value of 2 for STP_{185km}, a large probability difference (~70%) for an EF2-5 event is noted between weak (30 kt) and very strong (90 kt) 0.5° peak V_{rot} signatures. Comparatively, a smaller probability difference (~20%) is manifest between low STP_{185km} (i.e., ≤1) and very high STP_{185km} (i.e.,12) at a constant 0.5° peak V_{rot} of 60 kts. The apparent slight decrease in conditional tornado damage probabilities as STP_{185km} increases beyond values of 12 is likely a function of small sample size on the extreme upper-end of the distribution.

b. Operational application for diagnosing tornado intensity probability and IBW threat tag usage

A substantial percentage of EF2-5 events exhibit 0.5° peak V_{rot} values less than 60 kts (Fig. 6) even though EF2-5 events attain a higher conditional probability (i.e. 50%) than EF0-EF1 events at that value (Fig. 4). There is substantial overlap in EF-scale distribution in the 45-59.9 kt range (Figs. 6-7). In order to better diagnose more EF2-5 events with 0.5° peak V_{rot} below 60 kt, consideration of the near-storm environment, mode, and forecaster experience will likely be needed because 565 of 827 (68%) EF2-5 events had 0.5° peak V_{rot} less than 60 kt. The forecaster role in this process is to use all of the information at his/her disposal to best anticipate when EF2+ tornadoes are more likely within the range of 0.5° peak V_{rot} values (i.e., 45 kt – 59.9 kt) where substantial overlap of EF1 and EF2 tornadoes occur.

Several case examples of past tornado events are provided below to demonstrate the process of diagnosing conditional tornado intensity given the existence of a tornado. Tornado intensity estimation using the EF-scale as a suitable proxy is needed for each case and is illustrated for the first case in Figs. 8-11. SPC mesoanalysis plots of STP are provided for each case, with the additional values derived from a nearby observed sounding intended to allow for a qualitative assessment of the representativeness of each STP value. Also, radar-attribute information (reflectivity, 0.5° peak V_{rot} value) is shown to illustrate the use of a simplified multi-platform assessment of the situation. Additional information such as tornado location with respect to population density and damage indicator (DI) distribution are not provided for brevity. For example, in Case 1, the 8.2 STP_{185km} SPC mesoanalysis value is binned in the 8.00-9.99 STP bin and annotated relative to climatology in Fig. 9. Based solely on STP, conditional probabilities for

the three EF-scale classes are the following: EF0-1 (69%), EF2-5 (31%), and EF4-5 (6%). Similarly for 0.5° peak V_{rot} (Fig. 10), conditional probabilities are the following: EF0-1 (80%), EF2-5 (20%), and EF4-5 (0.4%). Combining both data types (Fig. 11) in a conditional probability distribution yield the following: EF0-1 (~62%), EF2-5 (~38%). Utilizing the figures presented in this paper (i.e., Figs. 3-5), consider how this information could be applied for IBW warning tags [i.e., base tier–no tag (EF0-1 events), considerable tag (EF2-5 events), catastrophic tag (EF4-5 events)] for the following cases.

CASE 1 (Figs. 8-11).

- Environment
  - 6.6 STP observed raob
  - 8.2 STP_{185km} SPC mesoanalysis
- Convective mode
  - Supercell
- 0.5° peak V_{rot}
  - 49 kt

CASE 2 (Fig. 12).

- Environment
  - 1.1 STP observed raob
  - 1 STP SPC mesoanalysis
- Convective mode
  - Supercell
- 0.5° peak V_{rot}
  - 35 kt

CASE 3 (Fig. 13).

- Environment
  - 4.9 STP observed raob
  - 6 STP SPC mesoanalysis
- Convective mode
  - Supercell
- 0.5° peak V_{rot}
  - 63 kt

CASE 4 (Fig. 14).

- Environment
  - 13.9 STP observed raob
  - 11 STP SPC mesoanalysis
- Convective mode
  - Supercell
- 0.5° peak V_{rot}
  - 82 kt

CASE 5 (Fig. 15).

- Environment
  - 0.9 STP observed raob
  - 1.6 STP_{185km} SPC mesoanalysis
- Convective mode
  - Supercell
- 0.5° peak V_{rot}
  - 32 kt

CASE 6 (Fig. 16).

- Environment
  - 6.7 STP observed raob
  - 13.7 STP_{185km} SPC mesoanalysis
- Convective mode
  - Supercell
- 0.5° peak V_{rot}
  - 92 kt

CASE 7 (Fig. 17).

- Environment
  - 10.1 STP observed raob
  - 8 STP SPC mesoanalysis
- Convective mode
  - Supercell
- 0.5° peak V_{rot}
  - 89 kt

CASE 8 (Fig. 18).

- Environment
  - 2.6 STP observed raob
  - 0 STP_{185km} SPC mesoanalysis
- Convective mode
  - QLCS
- 0.5° peak V_{rot}
  - 38 kt

A brief summary of the tornadoes for each case is listed in Table 2.

c. Limitations and considerations for diagnosing tornado intensity

While the above cases provide a useful exercise to diagnose tornado intensity, exceptional events can occur in near-storm environments or 0.5° peak V_{rot} with low conditional probabilities from this study's climatology. For example, an EF4 event occurred in Richland County, ND exhibiting a 40 kt 0.5° peak V_{rot} sampled at 9500 ft ARL with a 4.8

STP_{185km}. Additionally, an EF0 event occurred in Texas County, OK exhibiting an 86 kt 0.5° peak V_{rot} sampled at 7500 ft ARL with a 2.4 value of STP_{185km}. Miscellaneous non-meteorological factors such as radar sampling issues, population density, and the non-uniform spatial distribution of DIs result in uncertainty for any particular event.

A recommended best-practices approach for short-term tornado hazard diagnosis considers the use of information about the 1) near-storm environment, 2) convective mode, 3) 0.5° peak V_{rot} and 4) indirect evidence using polarmetric radar (i.e., TDS signature; Ryzhkov et al. 2002, Schuur et al. 2004) or confirming evidence of a tornado (e.g., spotter, live video) as a unifying frame-of-reference.

Despite the promise of STP_{185km} as a relatively simple environmental diagnostic to assess the potential for tornadoes, there is no replacement for a thorough diagnosis of the spatiotemporal distribution of buoyancy, shear, and moisture. Furthermore, anticipating changes to the near-storm environment via air mass modification near boundaries, storm interactions, etc., provides an observational foundation for effective use of SPC mesoanalysis data.

Specific attention focused on relating the conditional tornado probabilities to the IBW tiered warning tags has been used experimentally by some NWS offices as of late 2014. The conditional tornado damage probabilities presented herein are based in a large and diverse sample of events, which provides a valuable frame-of-reference for comparing individual events. While the conditional probability approach is NOT intended explicitly for tornado warnings with *lead time*, the STP_{185km} and 0.5° peak V_{rot} can aid in anticipating decision thresholds as the warning decision-making process evolves.

Future work may include exploring the utility of associating 0.5° peak rotational velocity data to Warning Decision Support System–Integrated Information (WDSS-II; Lakshmanan et al. 2007) low-level rotation track data (i.e., 0–2 km AGL merged azimuthal shear) in association with the multi-year reanalysis of remotely sensed storms (MYRORSS) project (Cintineo et al. 2011). Other possible statistical methods or refinements to probabilistic decision aids related to IBW warning decision thresholds are worth further investigation.

ACKNOWLEDGEMENTS

The authors thank Israel Jirak (SPC) for helping to clarify thoughts and for providing a thorough review of this manuscript.

REFERENCES

Andra, D. L., Jr., 1997: The origin and evolution of the WSR-88D mesocyclone recognition nomogram. Preprints, *28th Conf. on Radar Meteor*., Austin, TX, Amer. Meteor. Soc., 364–365.

Benjamin, S. G., and Coauthors, 2004: An hourly assimilation-forecast cycle: The RUC. *Mon. Wea. Rev*., **32**, 495–518.

Bothwell, P. D., J. A. Hart, and R. L. Thompson, 2002: An integrated three-dimensional objective analysis scheme in use at the Storm Prediction Center. Preprints, *21st Conf. on Severe Local Storms*, San Antonio, TX, Amer. Meteor. Soc., J117–J120. [Available online at https://ams.confex.com/ams/pdfpapers/47482.pdf].

Brady, R. H., and E. J. Szoke, 1989: A case study of nonmesocyclone tornado development in northeast Colorado: similarities to waterspout formation. *Mon. Wea. Rev.*, **117**, 843–856.

Brotzge, J. A., S. E. Nelson, R. L. Thompson, and B. T. Smith, 2012: Tornado probability of detection and lead time as a function of convective mode and environmental parameters. *Wea. Forecasting*, 28, 1261-1276.

Cintineo, J., T. Smith, V. Lakshmanan, and S. Ansari, 2011: An automated system for processing the multi-year reanalysis of remotely sensed storms (MYRORSS). Preprints, *27th Conf. on Interactive Information Processing Systems (IIPS)*, *91st Amer. Meteor. Soc. Annual Meeting*, Seattle, WA, J9.3.

Coniglio, M. C., 2012: Verification of RUC 0–1-km forecasts and SPC mesoscale analyses using VORTEX2 soundings. *Wea. Forecasting*, **27**, 667-683.

Crum, T. D., R. L. Alberty, and D. W. Burgess, 1993: Recording, archiving, and using WSR-88D data. *Bull. Amer. Meteor. Soc*., **74**, 645–653.

Dean, A.R., R.S. Schneider, and J.T. Schaefer, 2006: Development of a comprehensive severe weather forecast verification system at the Storm

Prediction Center. *Preprints*, 23nd Conf. Severe Local Storms, St. Louis, MO.

French, M. M., H. B. Bluestein, I. PopStefanija, C. A. Baldi, and R. T. Bluth, 2013: Reexamining the vertical development of tornadic vortex signatures in supercells. *Mon. Wea. Rev.*, **141**, 4576–4601.

Kingfield, D. M., J. G. LaDue and K. L. Ortega, 2012: An evaluation of tornado intensity using velocity and strength attributes from the WSR-88D mesocyclone detection algorithm. Preprints, *26th Conf. on Severe Local Storms*, Amer. Meteor. Soc., 3.2. [Available online at https://ams.confex.com/ams/26SLS/webprogram/Manuscript/Paper211488/Kingfield-etal-SLS2012-Peak_MDA_and_Tornado_Intensity.pdf].

LaDue, J. G., K. Ortega, B. Smith, G. Stumpf, and D. M. Kingfield, 2012: A comparison of high resolution tornado surveys to doppler radar observed vortex parameters: 2011-2012 case studies, Preprints, *26th Conf. on Severe Local Storms*, Nashville, TN, Amer. Meteor. Soc., 6.3. [Available online at https://ams.confex.com/ams/26SLS/webprogram/Manuscript/Paper212627/Hi-res-tornado-nowcasting2-20121205hi-qual.pdf].

Laflin, J. M., 2013: Verification of RAP model soundings in preconvective environments. *J. Operational Meteor.*, **1** (6), 66–70.

Lakshmanan, V., T. M. Smith, G. J. Stumpf, and K. Hondl, 2007: The Warning Decision Support System–Integrated Information. *Wea. Forecasting*, **22**, 596–612.

Mitchell, E. D., S. V. Vasiloff, G. J. Stumpf, A. Witt, M. D. Eilts, J. T. Johnson, and K. W. Thomas, 1998: The National Severe Storms Laboratory tornado detection algorithm. *Wea. Forecasting*, **13**, 352–366.

NOAA, 2011: NWS Central Region Service Assessment: Joplin, Missouri, Tornado, May 22, 2011. [Available online at http://www.nws.noaa.gov/om/assessments/index.shtml].

Parker, M. D., 2014: Composite VORTEX2 supercell environments from near-storm soundings. *Mon. Wea. Rev.*, **142**, 508–529.

Potvin, C. K., K. L. Elmore, and S. J. Weiss, 2010: Assessing the impacts of proximity sounding criteria on the climatology of significant tornado environments. *Wea. Forecasting* **25**, 921–930.

Ripberger, J. T., C. L. Silva, H. C. Jenkins-Smith, and M. James, 2014: The influence of consequence-based messages on public responses to tornado warnings. *Bull. Amer. Meteor. Soc,* in press.
doi: http://dx.doi.org/10.1175/BAMS-D-13-00213.1

Ryzhkov, A. V., D. W. Burgess, D. S. Zrnic, T. Smith, and S. E. Giangrande, 2002: Polarimetric analysis of a 3 May 1999 tornado. Preprints, *21st Conf. on Severe Local Storms,* San Antonio, TX, Amer. Meteor. Soc., 515–518.

Schuur, T. J., A. V. Ryzhkov, D. W. Burgess, and D. S. Zrnic, 2004: Polarimetric radar observations of tornadic debris signatures. Preprints, *22nd Conf. on Severe Local Storms,* Hyannis, MA, Amer. Meteor. Soc., CD-ROM, 8B.3.

Smith, B. T., R. L. Thompson, J. S. Grams, and J. C. Broyles, 2012a: Convective modes for significant severe thunderstorms in the contiguous United States. Part I: Storm classification and climatology. *Wea. Forecasting*, 27, 1114–1135.

_____, _____, H.E. Brooks, A.R. Dean, and K.L. Elmore, 2012b: Diagnosis of conditional maximum tornado probabilities. Preprints, *26th Conf. on Severe Local Storms*, Nashville, TN, Amer. Meteor. Soc., P2.20.

_____, _____, and A. R. Dean, 2014: The Storm Prediction Center tornadic storm and environment database: development and application. Preprints, *26th Conf. on Severe Local Storms*, Madison, WI, Amer. Meteor. Soc.,17.1.

Speheger, D. A., and R. D. Smith, 2006: On the imprecision of radar signature locations and storm path forecasts. *Natl. Wea. Dig.*, **30**, 3–10.

Stumpf, G. J., A. Witt, E. D. Mitchell, P. L. Spencer, J.T. Johnson, M. D. Eilts, K. W. Thomas, and D. W. Burgess, 1998: The National Severe Storms Laboratory mesocyclone detection algorithm for the WSR-88D. *Wea. Forecasting*, **13**, 304–326.

Thompson, R. L., R. Edwards, J.A. Hart, K.L. Elmore and P.M. Markowski, 2003: Close proximity soundings within supercell environments

obtained from the Rapid Update Cycle. *Wea. Forecasting*, **18**, 1243–1261.

_____, B. T. Smith, J. S. Grams, and C. Broyles, 2012: Convective modes for significant severe thunderstorms in the contiguous United States. Part II: Supercell and QLCS tornado environments. *Wea. Forecasting*, **27**, 1136–1154.

_____, _____, A. R. Dean, and P. T. Marsh, 2013: Spatial distributions of tornadic near-storm environments by convective mode. *Electronic J. Severe Storms Meteor.*, **8** (5), 1–22.

Torres, S. M., and C. D. Curtis, 2007: Initial implementation of super-resolution data on the NEXRAD network. Preprints, *23rd Int. Conf. on Interactive Information Processing Systems,* San Antonio, TX, Amer. Meteor. Soc., 5B.10. [Available online at http://ams.confex.com/ams/pdfpapers/116240.pdf]

Toth, M., R. J. Trapp, J. Wurman, K. A. Kosiba, 2013: Comparison of mobile-radar measurements of tornado intensity with corresponding WSR-88D measurements. *Wea. Forecasting*, **28**, 418–426.

Trapp, R. J. and M. L. Weisman, 2003: Low-Level mesovortices within squall lines and bow echoes. Part II: Their genesis and implications. *Mon. Wea. Rev.*, **131**, 2804–2823.

——, S. A. Tessendorf, E. S. Godfrey, and H. E. Brooks, 2005: Tornadoes from squall lines and bow echoes. Part I: Climatological distribution. *Wea. Forecasting*, **20**, 23–34.

Wagenmaker, R., Mann G., and Hudson M., 2014: NWS Central Region Impact-Based Warning project introduction and overview. [Available online at http://www.crh.noaa.gov/images/dtx/GLOMW/Presentations/2014_IBW_Project_Intro_Overview.pdf].

Wood, V. T. and R. A. Brown, 1997: Effects of radar sampling on single-doppler velocity signatures of mesocyclones and tornadoes. *Wea. Forecasting*, **12**, 928–938.

Table 1. Impact-based warning tiers for tornado warnings.

Tornado Warning Damage Threat Tags	
No Tag	Possible damage and generally a short-lived tornado
TORNADO DAMAGE THREAT… CONSIDERABLE	Credible observational evidence that a stronger variety tornado (EF2+) is imminent or ongoing. Tornado duration generally longer-lived.
TORNADO DAMAGE THREAT… CATASTROPHIC	DIRECT observational evidence that a stronger variety tornado (EF4-EF5) is striking or about to strike a population footprint with 100% certainty. Tornado duration generally long-lived. ***FAR will be zero.

Table 2. Tornado cases with corresponding tornado attributes.

	EF-rating	Event description
Case #1	2	26 Apr 2011 — Harrison Co., TX — 5.1 mi path, 400 yd wide
Case #2	1	08 July 2014 — Mercer Co., PA — 2.5 mi path, 150 yd wide
Case #3	2	11 May 2014 — Lancaster Co., NE — 2.5 mi path, 300 yd wide
Case #4	4	16 June 2014 — Stanton Co., NE — 12.1 mi path, 400 yd wide
Case #5	0	01 June 2012 — BWI Airport, MD — 6.6 mi path, 100 yd wide
Case #6	1	14 Apr 2012 — Harper Co., KS — 22.3 mi path, 1000 yd wide
Case #7	4	27 Apr 2014 — Mayflower/Vilonia, AR — 41.1 mi path, 1320 yd wide
Case #8	0	03 May 2009 — Madison Co., MS — 0.9 mi path, 100 yd wide

Figures

Figure 1. Spatial plot of tornado events by EF-scale (2009-2013).

Figure 2. A) WSR-88D base reflectivity (dBZ, color scale on left) at 0.5º beam tilt from Jackson, MS (KDGX) at 0852 UTC on 30 November 2010. A cluster RM produced an EF2 tornado in Smith County MS (start time 0844 UTC). North is up; county borders are black; distance scale (lower right). **B)** Same as Fig. 1A, except for storm relative velocity (kt, scale on left), 45 degree angle insert, and curved arrows signifying rotation. Denoted inserts display maximum inbound storm relative velocity (max V_{in}, 48.6 kt), maximum outbound storm relative velocity (max V_{out}, 30.1 kt), maximum rotational velocity (max V_{rot}, 39.4 kt).

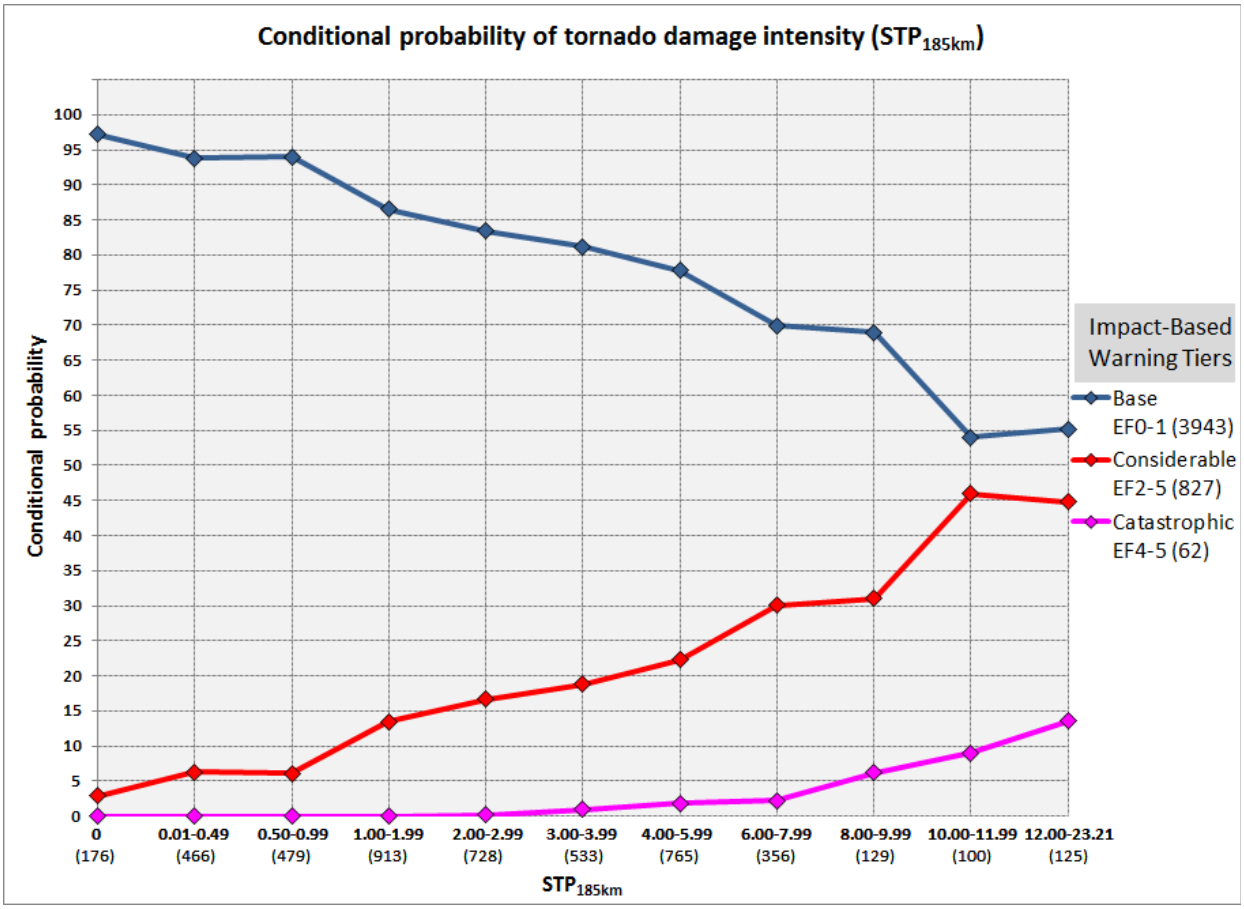

Figure 3. Conditional probabilities of meeting or exceeding grouped EF-scale rating classes with corresponding Impact-Based Warning tiers [legend; right: (EF0-EF1, Base; EF2-EF5, Considerable; EF4-EF5, Catastrophic)] for binned values of STP_{185km} [dimensionless; x-coordinate, (sample size)] for all convective mode tornado events [2009-2013; ≤ 10000 ft above radar level (ARL), 1–101 mi radius].

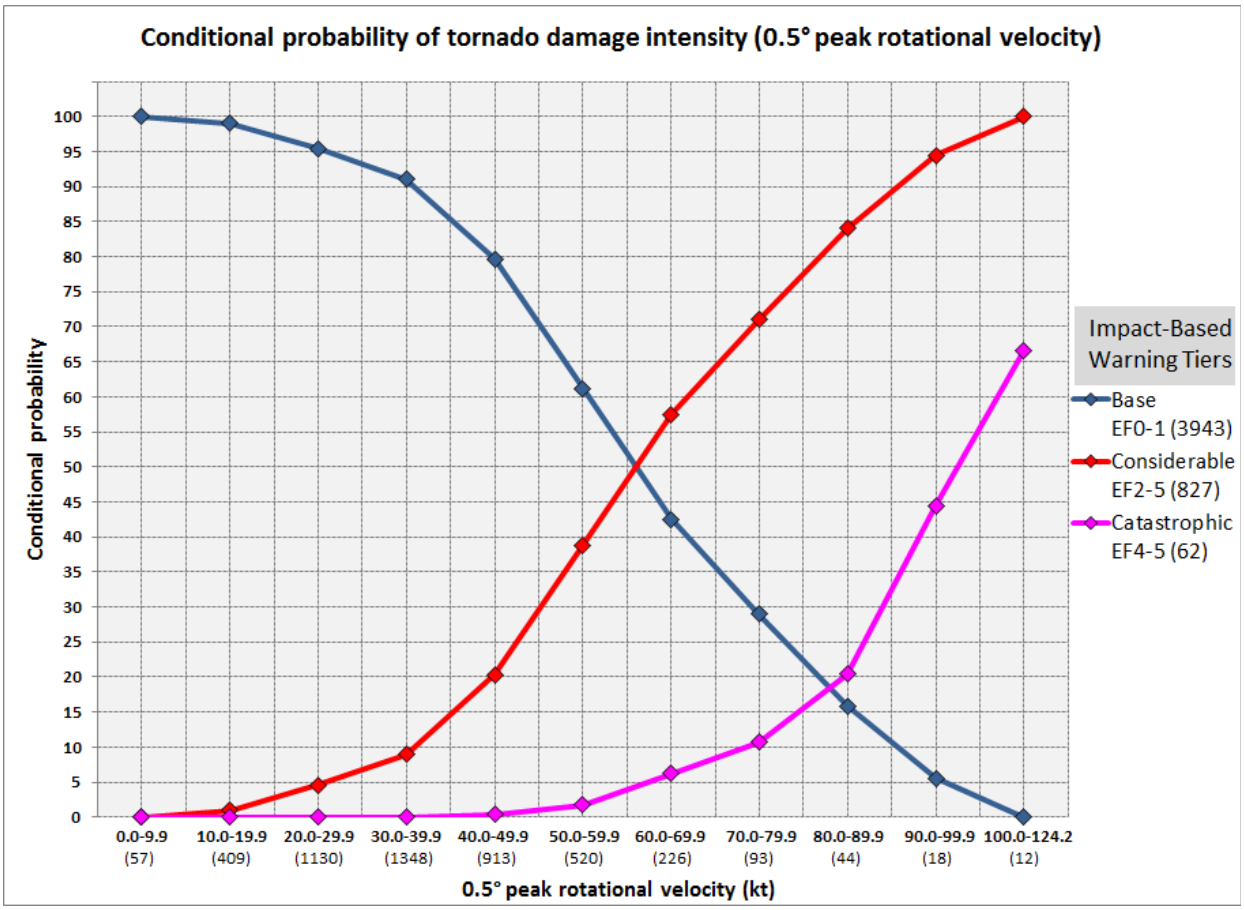

Figure 4. Same as Fig. 3 except for 0.5 degree peak rotational velocity (kt, x-coordinate).

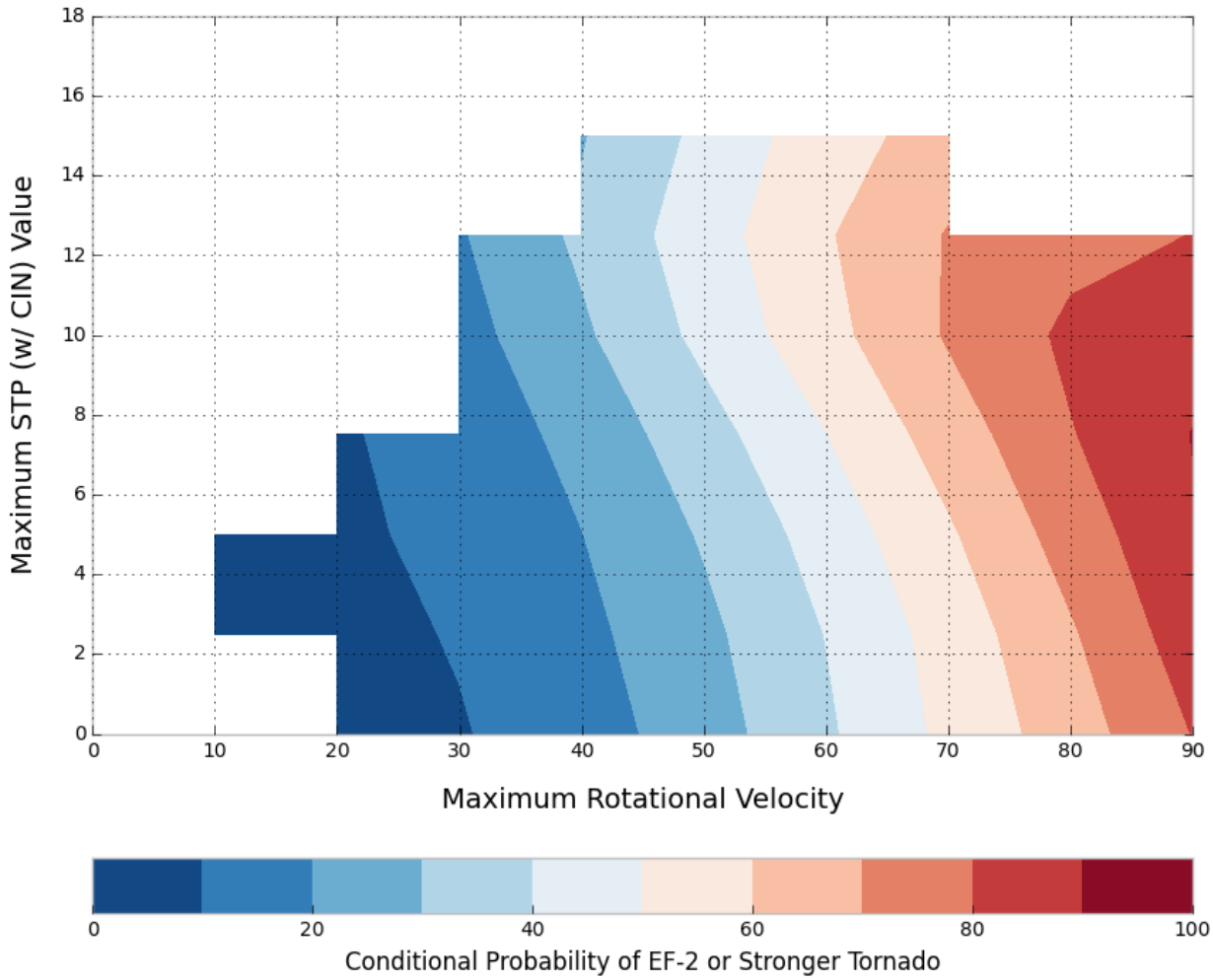

Figure 5. Smoothed conditional probability of EF2+ tornado rating (shaded) of 0.5 degree peak rotational velocity (kt, x-coordinate) vs. STP_{185km} (dimensionless, y-coordinate). The conditional probability is only calculated and shown for bins with at least one EF2+ tornado.

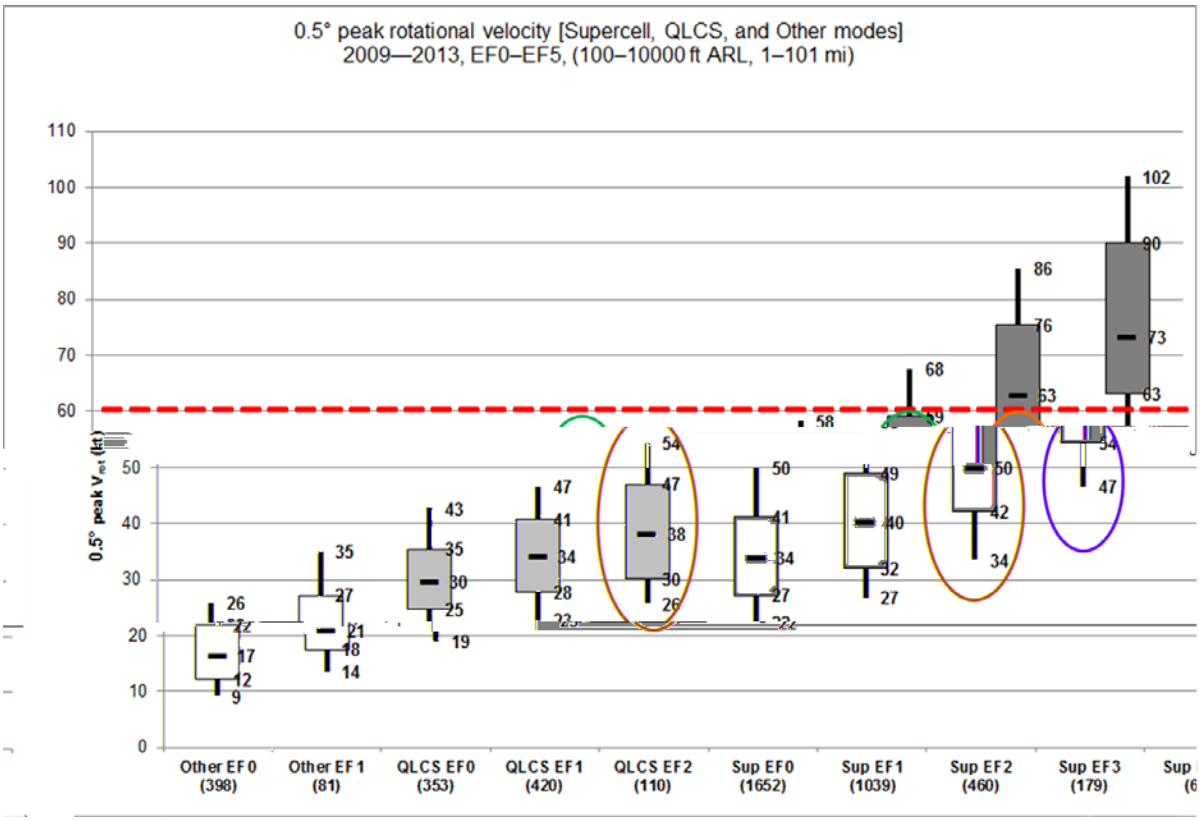

Figure 6. Box and whiskers plot of 0.5 degree peak rotational velocity (kt) of EF0–EF5 tornado events (2009–2013; ≤ 10000 ft ARL, 1–101 mi radius) grouped by supercell (Sup;dark gray), QLCS [(light gray) EF3 events not shown], and other modes (Other;white). The shaded boxes span the 25th to the 75th percentiles, and the whiskers extend upward to the 90th and downward to the 10th percentiles. Median values are marked within the box, and sample sizes for each storm mode and EF-scale category are shown in parentheses. Annotated in the red dashed line represents the 60 kt 0.5 degree peak rotational velocity threshold below which a substantial percentage of EF2 (green ellipsoid) and EF3 events are located.

Figure 7. Scatterplot of EF0–EF5 tornado events (2009-2013; inverted triangle symbol) by EF-scale rating (legend; top right) of 0.5 degree peak rotational velocity (kt) vs. STP_{185km} (dimensionless)] and 0.5 degree peak rotational

velocity proportionately sized to velocity strength. The circles represent the mean values of STP_{185km} and 0.5 degree peak rotational velocity for each EF-scale rating. The annotated green rectangle highlights tornado events with 0.5 degree peak rotational velocity of 45.0-59.9 kt.

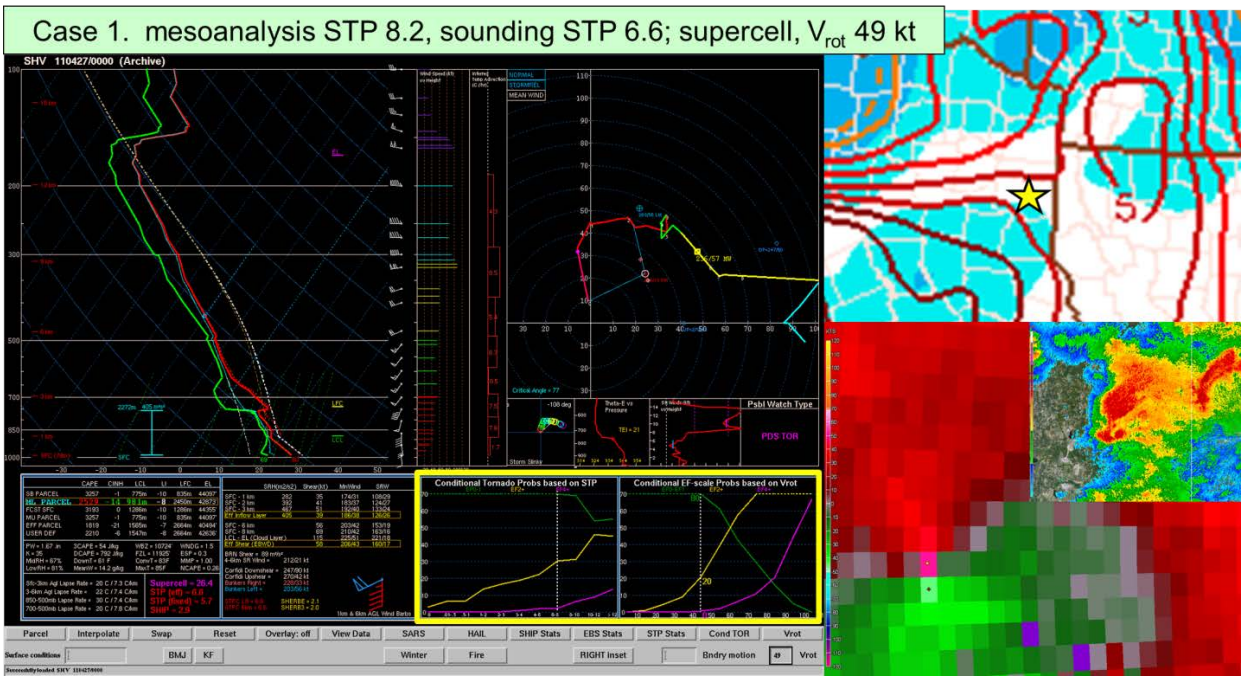

Figure 8. Case 1 (labeled top) with mesoanalysis STP_{185km} (8.2), sounding STP (6.6), supercell convective mode, and 0.5° peak rotational velocity [(V_{rot}) 49 kt]. Lower left, an observed proximity sounding display with annotated yellow rectangle highlighting conditional tornado probabilities for STP and 0.5° peak rotational velocity. Lower right . 0.5° storm rotational velocity and middle right (0.5° base reflectivity). Top right mesoanalysis STP with annotated yellow star depicting event location.

Figure 9. As in Fig. 3, but annotated (black dashed line) on the 8.00-9.99 bin for the Case 1 STP_{185km} (8.2) value.

Figure 10. As in Fig. 3, but annotated (black dashed line) on the 40.0-49.9 kt bin for the Case 1 0.5° peak rotational velocity (49 kt).

Figure 11. As in Fig. 5, but annotated (yellow star) for the Case 1 STP_{185km} (8.2) value and 0.5° peak rotational velocity (49 kt).

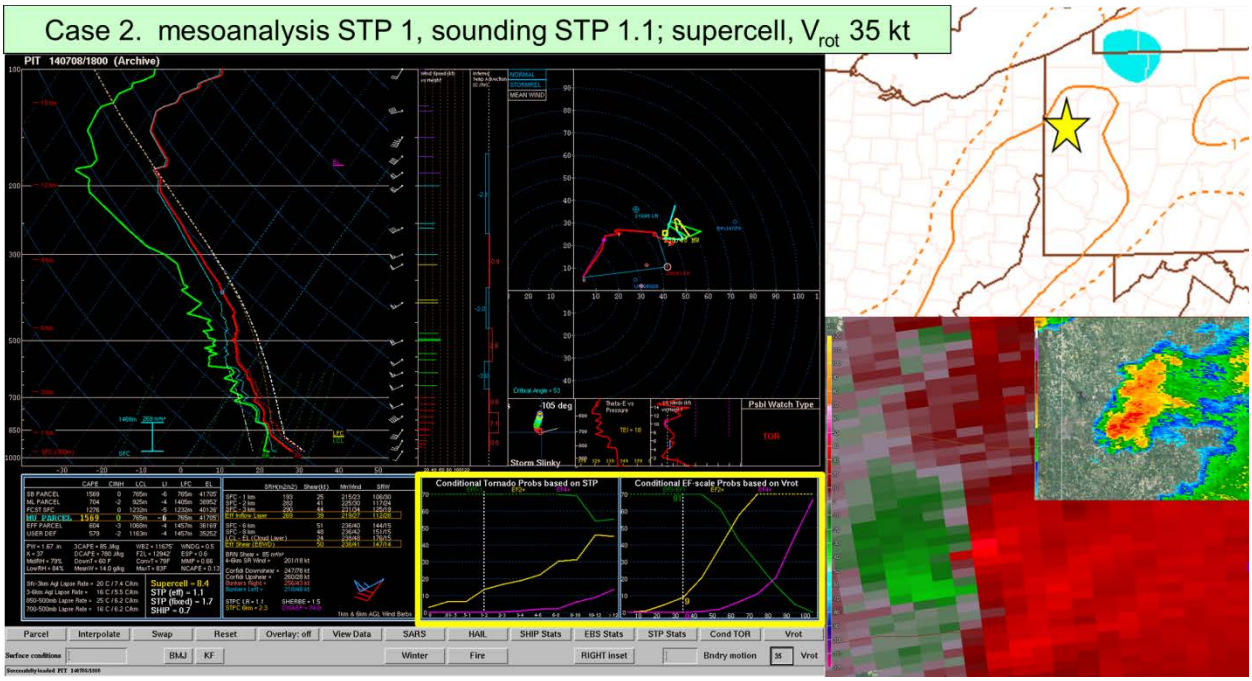

Figure 12. As in Fig. 8, but with mesoanalysis STP (1), sounding STP (1.1), and 0.5° peak rotational velocity [(V_{rot}) 35 kt].

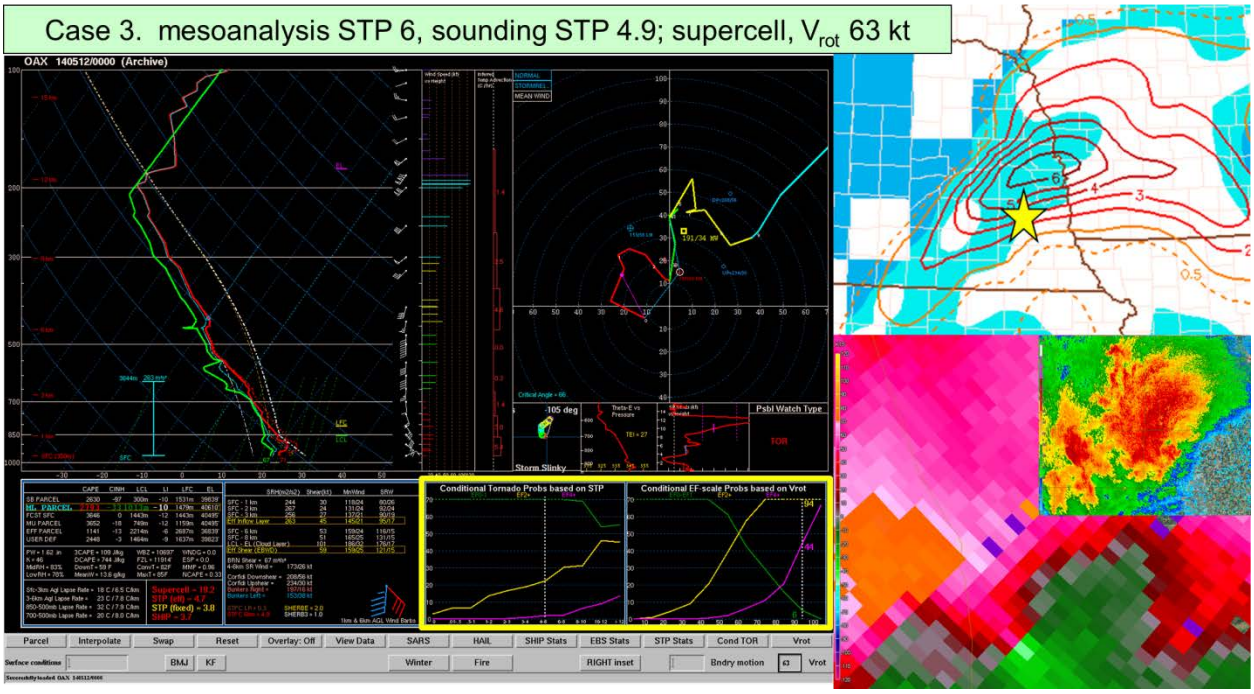

Figure 13. As in Fig. 12, but with mesoanalysis STP (6), sounding STP (4.9), and 0.5° peak rotational velocity [(V_{rot}) 63 kt].

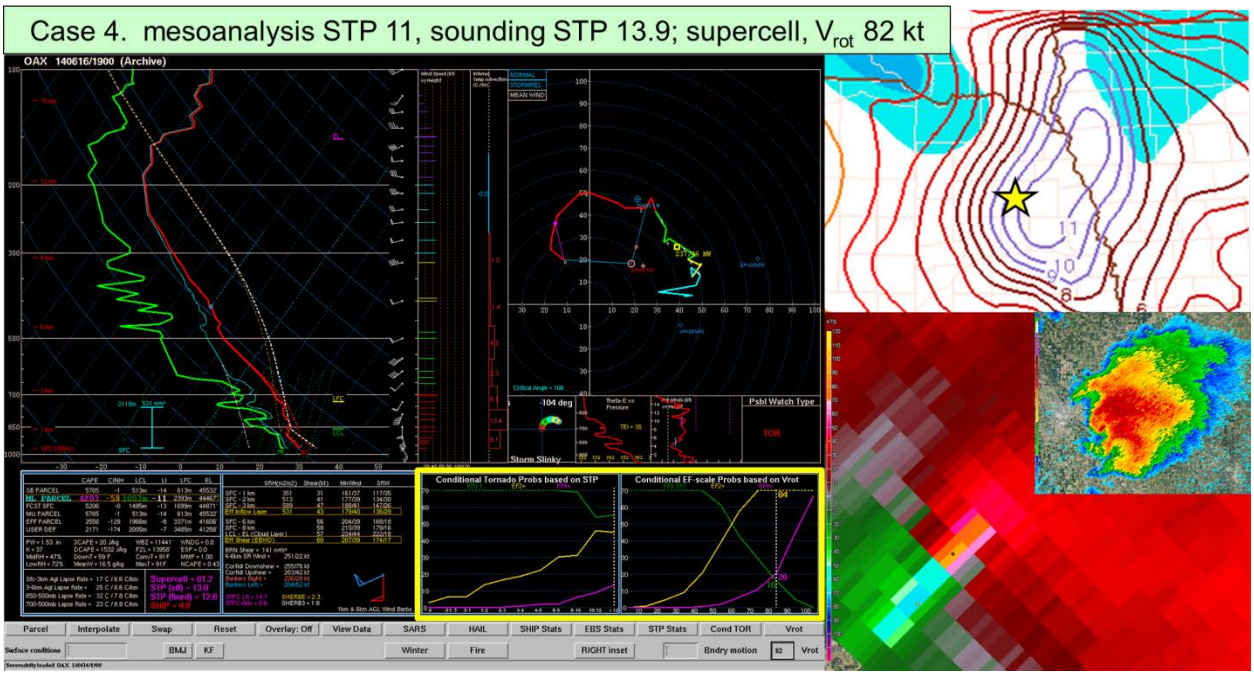

Figure 14. As in Fig. 12, but with mesoanalysis STP (11), sounding STP (13.9), and 0.5° peak rotational velocity [(V_{rot}) 82 kt].

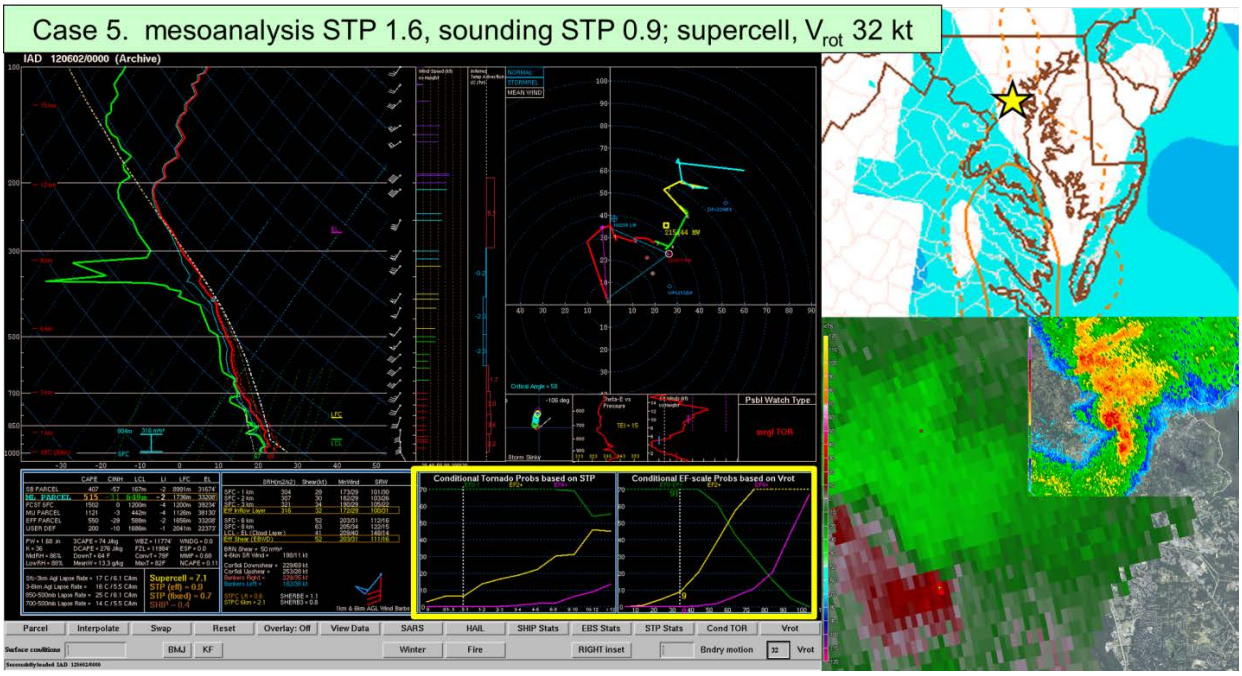

Figure 15. As in Fig. 8, but with mesoanalysis STP_{185km} (1.6), sounding STP (0.9), and 0.5° peak rotational velocity [(V_{rot}) 32 kt].

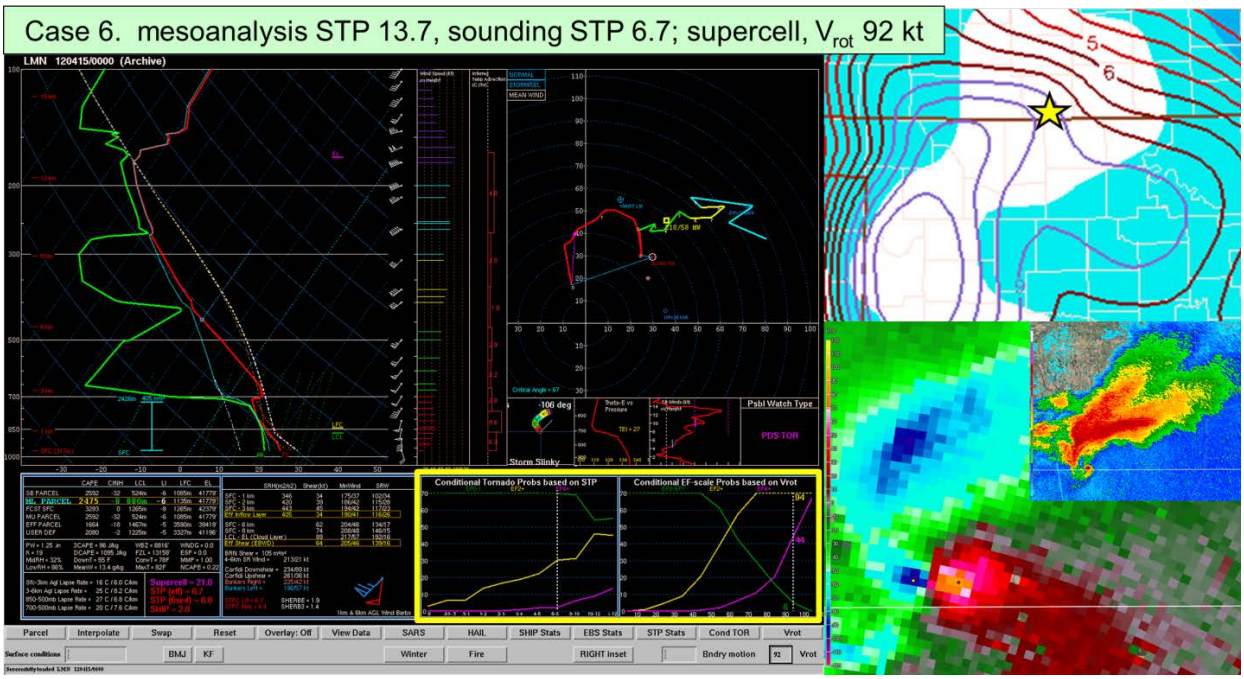

Figure 16. As in Fig. 8, but with mesoanalysis STP_{185km} (13.7), sounding STP (6.7), and 0.5° peak rotational velocity [(V_{rot}) 92 kt].

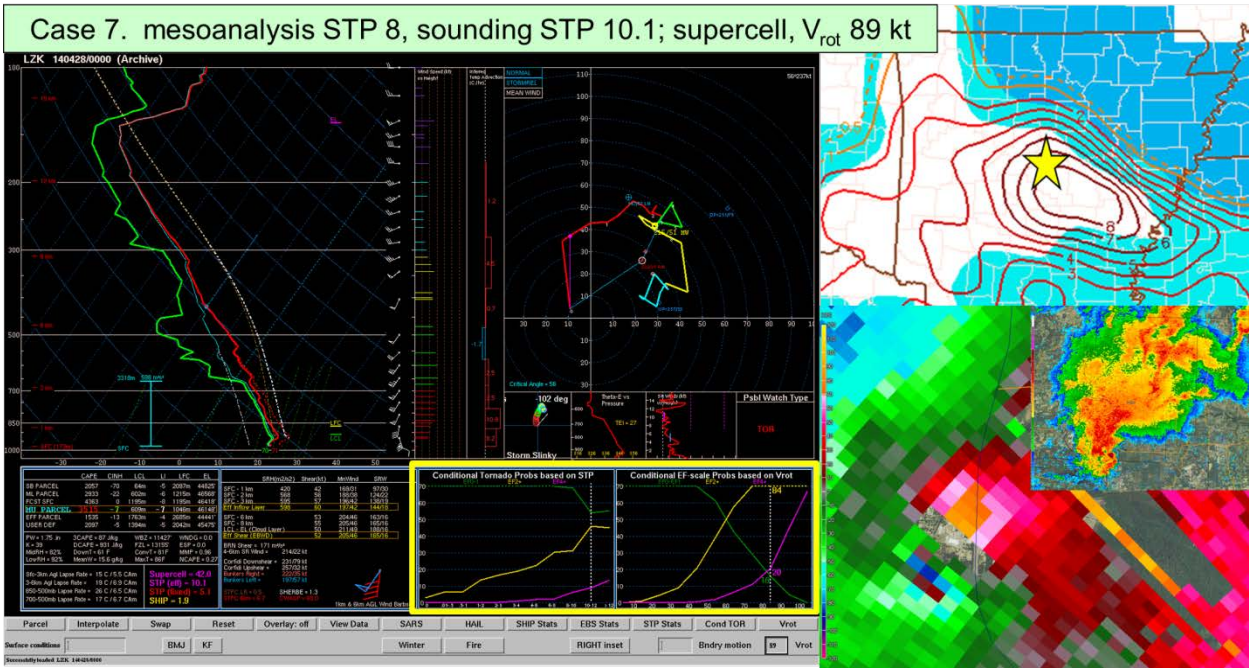

Figure 17. As in Fig. 12, but with mesoanalysis STP (8), sounding STP (10.1), and 0.5° peak rotational velocity [(V_{rot}) 89 kt].

Figure 18. As in Fig. 8, but with mesoanalysis STP_{185km} (0), sounding STP (2.6), and 0.5° peak rotational velocity [(V_{rot}) 38 kt].